A model for internal bores in continuous stratification

By BRIAN L. WHITE[1] AND KARL R. HELFRICH[2]

[1]Marine Sciences Department, UNC-Chapel Hill, NC, [2]Department of Physical Oceanography, Woods Hole Oceanographic Institution, Woods Hole, MA
bwhite@unc.edu, khelfrich@whoi.edu

(Received)

We describe a model for the speed of an internal bore as a function of amplitude in continuous stratification of arbitrary form. The model, an advancement over existing theories limited to idealized two-layer stratification, is based on a jump closure developed from the theory of nonlinear internal waves in continuous stratification. As such, the model accurately predicts bore speeds that are consistent in both the small- and large-amplitude limits with the properties of the ambient waveguide. Navier-Stokes simulations of both undular and turbulent internal bores produced by dam-break in ambient stratification of various forms show good agreement with model predictions. In nearly two-layer stratification with a finite pycnocline, the continuous model predicts a slower bore speed and more closely matches numerical results than existing two-layer theories. While the model requires an assumption for the structure of the energy dissipation, a closure is introduced which consistently produces good agreement with numerical results. This closure also sheds light on two-layer bore theories and leads to a new closure in that limit. We conclude that the properties of the nonlinear waveguide created by continuous stratification is critical in determining the bore speed, and additionally, gives physical insight into shape and character of the bore front.

1. Introduction

Internal bores, propagating hydraulic jumps, are common in the atmosphere and ocean and are important for turbulent mixing, mass and momentum transport, and even biological processes. A famous example is the Morning Glory in the Gulf of Carpentaria, an atmospheric undular bore generated by sea-breeze fronts (Rottman & Simpson 1989). In the ocean, internal bores are associated with river plume fronts (Nash & Moum 2005), flow over topography (Cummins *et al.* 2003) and shoaling internal tides (Pineda 1999). Energy is generally lost through the jump, which results either in turbulent dissipation or the radiation of packets of rank-ordered solitary waves, the latter termed an undular bore. Existing theories, which relate the bore speed to its amplitude, have focused primarily on the limit of sharp two-layer stratification. However, in the ocean and atmosphere, nonuniform vertical density structure is common. Here we present a new closure for the front speed of an internal bore continuous stratification of arbitrary structure.

2. Internal bores: Previous theories

2.1. *Problem description*

We consider a propagating internal hydraulic jump connecting two regions of uniform flow, generated, for example, by a dam-break release of an initially discontinuous interface (see figure 1). The ambient region has density profile $\rho_a(z-\eta)$ and the flow through the bore has density $\rho(z)$ and velocity $U(z)$ in a frame of reference moving with speed, C_b, which is assumed constant (velocity is positive to the left in the moving frame). The isopycnal (streamline) displacement relative to the ambient is $\eta(z)$.

2.2. *Internal bores in two-layer stratification*

Several models have been proposed for the two-layer limit which predict the bore speed, C_b, as a function of the interface location in the ambient, d_o (measured from the bottom), and the bore height, d_1. To obtain jump conditions, mass and momentum conservation are laws are enforced in each layer separately. However, an additional assumption is required to obtain an expression for the pressure jump across the bore. Several closures have been proposed, based on assumptions about the distribution of pressure (Yih & Guha 1955), or more often on the energy dissipation across the jump (see Baines 1995). The theory by Chu & Baddour (1977); Wood & Simpson (1984) (often termed CBWS) assumes that energy is conserved in the contracting layer and all dissipation occurs in the expanding layer. Klemp *et al.* (1997) (termed KRS) developed a closure that conserves energy in the expanding layer. The KRS closure reproduces the Benjamin (1968) gravity current front condition in the limit $d_o \to 0$, while that of CBWS does not. Li & Cummins (1998) (termed LC) detailed a more general theory in which the energy loss could be distributed arbitrarily between layers, yielding a family of solutions for the bore speed. Borden *et al.* (2012), in a numerical investigation of the energy budgets for two-layer bores, found that energy could be transferred from the upper to lower layer by turbulent mixing. In subsequent work (Borden & Meiburg 2013) they introduced a model to parameterize the turbulent mixing across the bore, enforcing conservation of vorticity (rather than energy), to produce a new closure for the front speed that produced better agreement with their numerical results. These theories each assume steady flow in a frame moving with the bore. Esler & Pearce (2011) investigated unsteady undular bores using an extension of Whitham (1974) modulation theory applied to a fully nonlinear, weakly dispersive internal wave model. We return to a discussion of two-layer theories in §3 after first discussing our continuous model.

2.3. *Nonlinear internal waves and conjugate states in continuous stratification*

To develop our theory, we view an internal bore as a limiting form of a nonlinear solitary wave, which can be described by the Dubreil-Jacotin-Long (DJL) equation (Dubreil-Jacotin 1934; Long 1953; Stastna & Lamb 2002). In a frame of reference moving with the solitary wave speed, c, the streamline displacement, $\eta(x,z)$, measured relative to the ambient with density profile $\rho_a(z_a)$ where $z_a = z - \eta(x,z)$, is given by

$$\nabla^2\eta + \frac{N^2(z-\eta)}{c^2}\eta = 0, \tag{2.1}$$

subject to boundary conditions $\eta = 0$ at $z = 0, 1$ and $\eta \to 0$ as $x \to \pm\infty$. Here N is the Brunt-Väisälä frequency, $N^2 = -(g/\rho_o)d\rho_a/dz_a$, and ρ_o is a constant reference density. While (2.1) neglects ambient shear, it can be incorporated (see Stastna & Lamb 2002).

Lamb (2002) showed that the wave amplitude increases with c up to one of two limiting outcomes (depending on ambient stratification and shear): **(1)** overturning, which occurs when the local velocity matches the wave speed ($u = c$ in the lab frame). A necessary

condition for overturning is that N be nonzero at the boundary, i.e. $z = 0$ ($z = 1$) for waves of elevation (depression) (Lamb 2002); **(2)** DJL solutions become broad-crested and approach an infinite-wavelength solution that, in the half-plane, represents a energy-conserving bore (Brown & Christie 1998; Lamb & Wan 1998). In this limit, the flat isopycnals through the wave are said to be *conjugate* to those in the ambient, and we refer to this solution as the *conjugate state*. Lamb & Wan (1998) found conjugate state solutions for arbitrary stratification and shear. In the two-layer Boussinesq limit, Lamb (2000) showed that the conjugate state speed is $C_{cs} = 0.5(g'H)^{1/2}$, and the upstream pycnocline depth is found at mid-depth $h_{cs} = H/2$, both independent of d_o, recovering the energy-conserving CBWS and KRS two-layer solutions.

3. A theory for internal bores in continuous stratification

Because the the conjugate state is energy-conserving, only one solution exists for a given ambient density profile. To develop a theory for the bore speed as a function of amplitude, dissipation can be incorporated into the conjugate flow theory to produce a family of solutions for a given profile.

3.1. *Conservation equations*

The conservation equations for an internal jump in continuous stratification follow the development in Lamb & Wan (1998); Lamb & Wilkie (2004); White & Helfrich (2008). Referring to figure 1, we assume there exists a region behind the bore in which the flow is uniform in x, and the pressure hydrostatic. Considering nominally inviscid motion slightly modified by dissipation, Bernoulli's equation can be written in a frame moving with C_b, along a streamline between the ambient (where variables have subscript a) and the region behind the bore (without subscripts) as

$$\tfrac{1}{2}\rho_o C_b^2 + \rho_a(z_a) g z_a + p_a(z_a) = \tfrac{1}{2}\rho_o u(z)^2 + \rho_a(z-\eta) g z + p(z) + \Delta(z). \tag{3.1}$$

Here $\Delta(z)$ represents an energy head loss with arbitrary vertical structure. Here and subsequently, we make the Boussinesq approximation by assuming density variation is weak relative to a fixed reference value, ρ_o, and is therefore only important in the gravity term. Diffusion of density is also neglected, implying density isopycnals coincide with streamlines. By continuity, the velocity is related to the bore speed by $u(z) = C_b(\eta_z - 1)$. Hydrostatic pressure gives $dp/dz = -\rho_a(z-\eta)g$ and $dp_a/dz_a = -\rho_a(z_a)g$ through the bore and ambient regions, respectively. After (1) taking the vertical derivative, d/dz, of (3.1), (2) substituting the continuity and hydrostatic pressure relations, and (3) noting that a vertical derivative of any quantity is related to its derivative in the ambient by $d/dz = (1-\eta_z)d/dz_a$, an equation is obtained for the streamline displacement,

$$\eta_{zz} + \frac{N^2(z-\eta)}{C_b^2}\eta + \frac{\Delta_z}{\rho_o C_b^2(\eta_z - 1)} = 0, \tag{3.2}$$

which is subject to boundary conditions $\eta(0) = \eta(H) = 0$. This constitutes an eigenvalue problem for the bore speed, C_b and the streamline displacement, $\eta(z)$. In the linear limit $\eta \to 0$ and with $\Delta = 0$, (3.2) reduces to the linear equation governing normal modes in continuously-stratified Boussinesq fluid.

As with two-layer theories, conservation of momentum flux must also be enforced between the bore and ambient regions, resulting in an additional constraint,

$$\int_b \left[p(z) + \rho_o u^2(z)\right] dz = \int_a \left[p_a(z_a) + \rho_o C_b^2\right] dz_a. \tag{3.3}$$

Using (3.1) to write $p_a(z_a)$ in terms of $p(z)$ and again using $d/dz = (1-\eta_z)d/dz_a$, the hydrostatic relation, and integration by parts, yields

$$\int_0^H \left[\tfrac{1}{4}\rho_o C_b^2 \eta_z^3 - \left(1-\tfrac{1}{2}\eta_z\right)\Delta(z)\right] dz = 0. \tag{3.4}$$

In the special case $\Delta = 0$, (3.2) and (3.4) is equivalent to the conjugate state of Lamb & Wan (1998). The addition of the arbitrary $\Delta(z)$ term allows for a range of solutions, but requires an appropriate closure.

3.2. *Energy head loss*

We assume the head loss can be written as the product of a constant and a vertical shape function, $\Delta(z) = \Delta_o f(z)$. Given an assumption for $f(z)$, Δ_o (along with C_b) is part of the solution obtained from (3.2) and (3.4). The shape function distributes the head loss across isopyncals, and is the continuous analog of the two-layer closures that distribute dissipation arbitrarily between layers.

To illustrate, consider the following distribution which is linear in the non-dimensional density, or buoyancy, $b(z) = (\rho - \rho(H))/(\rho(0) - \rho(H))$,

$$\Delta(z) = \Delta_o f(z) = \Delta_o\left[\tfrac{1}{2} + \epsilon\left(b(z) - \tfrac{1}{2}\right)\right] \tag{3.5}$$

where $\Delta_o = \Delta(0) + \Delta(H)$ and $\epsilon = (\Delta(H) - \Delta(0))/\Delta_o$. Here $\Delta_o/2$ is the arithmetic mean head loss (and the loss on the mid-density isopycnal, $\Delta_o/2 = \Delta_{b=0.5}$), while ϵ measures the difference relative to the mean. The one-parameter family in ϵ distributes dissipative losses non-uniformly across isopycnals, and recovers the LC general theory in the two-layer limit, as illustrated by the following cases:

(a) $\epsilon = 1$. Here $\Delta(z) = \Delta_o b(z)$, confining the loss near the bottom expanding region. In two-layer limit, $b(z)$ is a step function and (3.5) is equivalent to the CBWS closure.

(b) $\epsilon = -1$. Here $\Delta = \Delta_o(1 - b(z))$, which distributes the head loss through the upper contracting region. In the two-layer limit, (3.5) is equivalent to the KRS solution.

(c) $\epsilon = 0$. Here $\Delta = \Delta_o/2 = constant$, which distributes the head loss uniformly. In the two-layer limit this is equivalent to the Borden & Meiburg (2013) vorticity conservation model (see §3.3).

(d) $\epsilon \to -\infty$. In this case, $\Delta(z) = \Delta_o\epsilon(b(z) - \frac{1}{2})$ and $\Delta(0) = -\Delta(H)$, implying energy is gained in the lower layer at the expense of the upper layer. Although $\Delta_o \to 0$, the product $\epsilon\Delta_o$ is finite, and it will be shown later that this solution results, perhaps counterintuitively, in a larger rate of total dissipation than the other special cases **(a)**-**(c)**.

In the two-layer limit, the general LC theory can be written in terms of ϵ,

$$\frac{C_b}{(g'H)^{1/2}} = \left[\frac{2d_oR^2(1-d_oR)^2\left(1-\epsilon(1-d_o-d_oR)\right)}{(d_oR^2-3d_oR+R+1)(1-d_oR)(1-\epsilon)+(d_oR^2-3d_oR+2)d_oR(1+\epsilon)}\right]^{1/2}, \tag{3.6}$$

where $R = d_1/d_o$ is the ratio of the bore height to the ambient interface height and $g' = g(\rho(0) - \rho(H))/\rho_o$. It can be verified that (3.6) recovers the CBWS and KRS solutions for $\epsilon = 1$ and $\epsilon = -1$, respectively. For continuous stratification, the structure of $\Delta(z)$ may be more complex. In §5 we compare (3.5) with profiles of dissipative losses from Navier-Stokes simulations.

With the head loss given by (3.5), the eigenvalue problem governing the conjugate bore (3.2) reduces to

$$\eta_{zz} + \frac{N^2(z-\eta)}{C_b^2}\left(\eta - \frac{\epsilon\Delta_o}{\rho_o g'}\right) = 0, \quad \eta(0) = \eta(H). \tag{3.7}$$

3.3. *Vorticity production*

If (3.2) is multiplied by C_b one then obtains a general statement about vorticity production downstream of the bore,

$$u_z = C_b \eta_{zz} = -\frac{N^2(z-\eta)}{C_b}\eta - \frac{1}{\rho_o C_b}\frac{d\Delta}{dz_a}. \tag{3.8}$$

Downstream vorticity arises from baroclinicity (first term on right) and gradients of dissipation across streamlines (lines of constant $C_b z_a$) (second term on right). In the absence of baroclinic effects this result has a well-known counterpart in rotating, single-layer shallow water flows where changes in potential vorticity q across a steady jump are related to gradients of the Bernoulli function across streamlines through $[q] = d[B]/d\psi$, where B is the Bernoulli function and ψ is the streamfunction (see §3.5 in Pratt & Whitehead 2008). When $\epsilon = 0$ in (3.5) the dissipation is the same along all streamlines and downstream vorticity arises solely from baroclinic effects. Thus the two-layer "vortex sheet" model of Borden & Meiburg (2013), which is based on vorticity production by baroclinic effects only, is recovered from (3.6) with $\epsilon = 0$.

3.4. *Energy dissipation*

The total rate of energy dissipation for a steady, Boussinesq, stratified bore, is given by the difference in energy flux between sections b and a, respectively, in figure 1,

$$D = \int_a C_b \left[p_a + \tfrac{1}{2}\rho_o C_b^2 + \rho_a(z-\eta)g z_a\right] dz_a - \int_b u\left[p + \tfrac{1}{2}\rho_o u^2 + \rho_a(z-\eta)gz\right] dz. \tag{3.9}$$

Through manipulations similar to those described in §3.1, (3.9) can be simplified to,

$$D = \int_0^H u(z)\Delta(z)dz = \int_0^H C_b(1-\eta_z)\Delta(z)dz. \tag{3.10}$$

where $D > 0$ implies a net energy loss, as required for a physically realistic bore solution. In the two layer limit, this expression reduces to $D = e_l + e_u$, the sum of the dissipation in the lower and upper layers, respectively, as given by the formulas (9) and (11) in Li & Cummins (1998). In terms of Δ_o and ϵ, $e_u = \Delta_o/2(1-\epsilon)(H-d_o)C_b$ and $e_l = \Delta_o/2(1+\epsilon)d_o C_b$. These expressions illustrate why $D > 0$ for $\epsilon \to -\infty$. Although $\Delta(z)$ is symmetric with $\Delta(0) = -\Delta(H)$, the positive head loss in the contracting layer is carried by a faster current, offsetting the energy gain in the lower layer.

3.5. *Trapped cores*

It is possible for (3.2) to develop solutions for which $z_a = z - \eta(z) < 0$, which implies, unphysically, that isopycnals originate from $z_a < 0$ (Lamb & Wan 1998; Stastna & Lamb 2002; Helfrich & White 2010). The onset of this condition occurs when $\eta_z = 1$, or $u(z) = 0$ in the wave frame. Lamb & Wilkie (2004) found solutions to the conjugate DJL equation beyond this limit by assuming a uniform trapped core of constant density $\rho = \rho_a(0)$ (for bottom-propagating waves) and Helfrich & White (2010) used a similar framework to find solutions to the full DJL equation (2.1) with a trapped core. In these methods, the flow must be matched along the core boundary with the DJL equation outside. A simpler approach, suggested by Helfrich & White (2010) and King *et al.* (2010), is to 'virtually' extend the ambient density profile $\rho_a(z_a)$ below $z_a = 0$ by smoothly and rapidly matching the stratification at the boundary to a uniform density region $\rho_a(-\infty)$, only slightly greater than $\rho_a(0)$, for $z - \eta < 0$. This results in a uniform density core with approximately zero circulation. For example,

$$N^2(z-\eta) = N^2(0)\exp\left[-((z-\eta)/\delta)^2\right], \quad z-\eta < 0. \tag{3.11}$$

Incorporating this approximation into (3.2) allows smooth solutions for $\eta(z)$ throughout the domain. We employ this approximation with $\delta = 0.01H$ only when $z - \eta < 0$ somewhere in the domain. In practice, this occurs only when $N^2(0) > 0$ (Lamb 2002).

3.6. *Numerical solution method*

The continuous model, (3.4) and (3.7), can be solved by a nested iterative approach as follows (from the inner- to outer-most levels): (1) Beginning with an initial value for $\eta_z(0) \equiv \eta_o'$, a proxy for the bore amplitude, find a value of C_b that satisfies the eigenvalue problem (3.7) by a shooting method. That is, integrate the ODE with initial values $\eta(0) = 0$, $\eta_z(0) = \eta_o'$, iterating on C_b until the upper boundary condition, $\eta(H) = 0$, is satisfied. (2) Iterate on η_o' until the bore amplitude, $h_b \equiv \int_0^H b(z)dz$ is equal to the desired value. (3) Iterate by varying the head loss constant, Δ_o, until the momentum conservation equation, (3.4), is satisfied.

4. Numerical Simulations

4.1. *Numerical Method and Setup*

To test the theory, numerical simulations were performed for internal bores released from a dam-break initial condition, with nominally two-layer stratification of varying interface thickness. We solve the two-dimensional Boussinesq Navier-Stokes equations,

$$\frac{\partial \mathbf{u}}{\partial t} + \mathbf{u}\cdot\nabla\mathbf{u} = -\nabla p - b\hat{\mathbf{k}} + \frac{1}{Re}\nabla^2\mathbf{u}, \qquad \nabla\cdot\mathbf{u} = 0, \qquad \frac{\partial b}{\partial t} + \mathbf{u}\cdot\nabla b = 0 \tag{4.1}$$

where p is the dimensionless pressure that remains after removing the hydrostatic part due to $\rho(H)$, b is the dimensionless buoyancy as defined in §3.2, and $\hat{\mathbf{k}}$ is the unit vector in the positive $z-$direction. Velocities are scaled by $\sqrt{g'H}$, lengths by H, time by $H/\sqrt{g'H}$, pressure by $\rho_o g'H$, and Re is the Reynolds number. Model results presented below are scaled in the same manner.

The numerical model uses a finite-volume discretization with a second-order pressure projection method based on that of Bell & Marcus (1992) and a Godunov-type advection scheme. This non-ocscillatory finite volume formulation is ideal for internal jumps with sharp gradients in density and velocity, and has been used to simulate gravity currents (White & Helfrich 2008, 2012), and nonlinear solitary waves (c.f. Lamb 2002), correctly capturing phase speeds and exhibiting minimal energy loss over large distances.

Calculations were done in a rectangular domain spanning, $-L/2 \le x \le L/2$ and $0 \le z \le H$, where $L = 32$, and and $H = 1$, with a resolution ($x \times z$) of 8192×256. Boundary conditions were free slip and a dam-break initial condition was used, with $\mathbf{u} = 0$ and an initial buoyancy field

$$\begin{aligned} b(x,z) &= (\hat{b} - \hat{b}(\infty,1))/(\hat{b}(\infty,0) - \hat{b}(\infty,1)) \\ \hat{b}(x,z) &= \tfrac{1}{2} - \tfrac{1}{2}\tanh\left[\lambda(z - z_o(x))\right] \\ z_o(x) &= \tfrac{1}{2}(h_d + d_o) - \tfrac{1}{2}(h_d - d_o)\tanh(\lambda x/2). \end{aligned} \tag{4.2}$$

This results in a virtual dam of height h_d, that transitions to an ambient (rescaled) density profile, $\rho_a(z) = \frac{1}{2} - \frac{1}{2}\tanh[\lambda(z - d_o)]$ with a nominal interface located at d_o and a thickness described by the parameter λ (thickness $\sim 1/\lambda$) (see figure 3, $t = 0$). Approximately 150 simulations were conducted spanning $\lambda = [4, 8, 12, 24, 64]$, $d_o = [0.1, 0.2, 0.3, 0.4]$ and a range of dam heights between $h_d = [0, 1]$ for each (λ, d_o) combination. The Reynolds number was 40,000, which ensured adequate resolution of the energy budget. While there is always a small amount of numerical dissipation, the resolved viscous dissipation,

globally integrated, was typically 85% of the total energy loss calculated from the residual of the kinetic energy budget.

4.2. *Internal bore properties*

In order to compare the theory with the numerical simulations, the bore speed, C_b and effective height, h_b were extracted from the results. The height is taken to be

$$h_b(x) = \int_0^H b(x, z, t)dz, \tag{4.3}$$

which makes the hydrostatic pressure behind the bore equivalent to that of a sharp two-layer bore of the same height. This definition was also used by Borden *et al.* (2012) for internal bores and by Marino *et al.* (2005) for the equivalent thickness of a gravity current. The mean height, $\overline{h}_b$, is the average value of $h_b(x)$ between $x = [0, x_f]$, where x_f is the front position, taken as the point at which the displacement is 1/4 of the maximum, $h_b(x_f) = \frac{1}{4}[h_{b_{max}} - \tilde{d}_o]$, where $\tilde{d}_o = h_b(L/2)$. The bore speed, C_b is calculated for each case by linear regression of x_f vs. t. From figure 2b it can be seen that the regression is highly linear; the uncertainty in C_b is generally less than 0.1% of its mean value.

Figure 3 shows the time evolution of an undular bore (a) and a turbulent bore (b) for $d_o = 0.2$ and $\lambda = 24$. The undular bore, which evolves from an initial dam height $h_d = 0.5$ is transient and continually radiates solitary-like waves from the front (c.f. Esler & Pearce (2011)). The turbulent bore, with initial dam height $h_d = 0.9$ exhibits a smooth monotonic front with Kelvin-Helmholtz vortices and turbulent mixing behind. While there is a continuum between these states, depending on h_d for a given $[\lambda, d_o]$, this dichotomy provides a reasonable means of classifying the simulations.

Figures 4 and 5 illustrate the effect of interface thickness, i.e. λ, on undular and turbulent bores. For undular bores, $d_o = 0.2$, $h_d = 0.5$, a decrease in interface thickness affects the rate of internal wave radiation, as an increasing number of crests with decreasing thickness (figure 4). For turbulent, or perhaps better termed monotonic, bores (figure 5), increasing interface thickness reduces the turbulent mixing, suppressing the Kelvin-Helmholtz instability entirely for the $\lambda = 4$ case. These results illustrate that a thicker interface reduces the energy dissipation rate of both undular and turbulent bores, discussed further in §5.2.

5. Comparison of simulations with theory

5.1. *Bore speed*

For comparison with the Navier-Stokes simulations, theoretical curves for $C_b(h_b)$ were generated over a range of (λ, d_o) values using the conjugate bore theory described in §3. The dissipation model (i.e. ϵ) was also varied. Results are shown in Figure 6 for $d_o = 0.1$ (a), 0.2 (b), 0.3 (c), and 0.4 (d). The KRS two-layer model is shown for comparison. Each model curve terminates at the energy-conserving conjugate state, $\Delta_o = 0$, which is independent of ϵ for a given (λ, d_o). Beyond the conjugate state, solutions are unphysical because $D < 0$. In general, the agreement between the model and the simulations is excellent. The model captures the behavior quite well for small bore amplitude, consistent with the ability of the DJL model to describe small-amplitude waves. For larger values of the ambient lower layer thickness ($d_o = 0.3, 0.4$) the agreement is ideal up to the conjugate state, and nearly independent of ϵ.

For $d_o = 0.1, 0.2$ the theory is more sensitive to the dissipation model, although the agreement with the simulations is still reasonable for most ϵ. The interface thickness has a greater influence on the front speed than the dissipation model. As with two-layer

bores, the continuous analog of the KRS model ($\epsilon = -1$) better captures the bore speed at large amplitude than the CBWS analog ($\epsilon = 1$). However, it is clear that the best agreement for all values of (λ, d_o) is found for $\epsilon \to -\infty$ model.

5.2. *Energy dissipation*

Some insight into the success of the $\epsilon \to -\infty$ model can be gained from the net dissipation, D, shown in Figure 6e,f for $\lambda = 12$, for $d_o = 0.1$ and 0.2. The $\epsilon \to -\infty$ model produces the greatest net dissipation as compared with the CBWS and KRS analogs, despite the energy gain in the lower layer, as discussed in §3.3 (representative of all values of λ). The higher rate of dissipation translates to the slowest bore speed (for solutions with $\Delta_o > 0$, up to the conjugate state), correcting the tendency of the other models to over predict C_b, which is also seen in the two-layer limit (see Borden *et al.* 2012).

The net dissipation was calculated from the simulations and is shown in figures 6e,f vs. the theory. The actual dissipation lies somewhere between the KRS analog and the $\epsilon \to -\infty$ limit. In figure 6g,h the simulation results are shown for a range of λ vs. the $\epsilon \to -\infty$ model curves. For $d_o = 0.1$ the agreement is reasonable and dissipation consistently increases with decreasing interface thickness. For $d_o = 0.3$,$\lambda = 64$ the simulations have much higher dissipation than any of the models. It is possible that the $\epsilon \to -\infty$ model produces the best agreement for C_b because it maximizes the dissipation.

5.3. *Bernoulli head loss*

From the simulations, we calculate the head loss in isopycnal coordinates from the Bernoulli function (3.1),

$$\Delta(b(x,z)) = \tfrac{1}{2}\left(C_b^2 - u^2 - w^2\right) - b\eta + p_a(z-\eta) - p, \tag{5.1}$$

where $u(x,z)$, $v(x,z)$, $p(x,z)$, and $b(x,z)$ are the local fields, $\eta(x,z) = z - z_a(b)$, and u is in the frame moving with C_b. We calculate the average $\Delta(b)$ between $[0, x_f]$ and between $t = [10, 32]$ for each simulation. Results are shown for undular and turbulent bores in figures 4 and 5 (middle panels) along with the linear regression for each case based on the model (3.5). The linear fit is reasonable (at least in the central region) for $\lambda = 24$, for both undular and turbulent bores. For the undular bores shown in figure 4, $\epsilon < -1$, consistent with a gain in energy in the lower layer. The thin-interface turbulent bores (e.g. $\lambda = 24$, figure 5) also gain energy in the lower layer, with $\epsilon < -1$. For the turbulent bores with a thicker interface ($d_o = 0.2$,$h_d = 0.5$,$\lambda = 4, 12$) the head loss is more complex. Near the bottom ($b = 1$), there is still energy gain, the best fit linear curve has $\epsilon < -1$. From figure 6, the model is less sensitive to ϵ for large amplitude bores, perhaps explaining why the $\epsilon \to -\infty$ model for still works well for C_b in this range.

5.4. *Velocity and density profiles*

It is instructive to compare the velocity and density profiles predicted by the model with profiles from the simulations. For example, the shear and stratification through the bore will influence the onset of shear instability and turbulent mixing. Mean profiles were calculated from the simulations by averaging over $x = [0, x_f]$, and vertically shifting to align local profiles with the mean bore thickness. That is we average $U(x, \tilde{z})$ and $b(x, \tilde{z})$, where $\tilde{z} = z - (h_b(x) - \overline{h}_b)$. The shift avoids interpreting undulations as enhancing pycnocline thickness, and also preserves local gradients, leaving shear and N^2 unaltered. Mean profiles of $U(z)$, $b(z)$, and the Richardson number, $Ri = N^2/(dU/dz)^2$, are shown in figures 4 and 5 (right panels) along with model predictions, using $\epsilon \to -\infty$. For the undular bores shown in figure 4, the model and simulations are almost indistinguishable. Here the Richardson number was always > 1, so it was not shown over the entire range.

For turbulent (or monotonic) bores (figure 5) the agreement is still quite good. The minimum Richardson number is well predicted by the model, and shear instabilities are well correlated with minimum Ri that approach 1/4.

5.5. *Internal waves at the front*

The transition from undular to monotonic bores with turbulent mixing, can be viewed as a continuum of solitary waves of increasing amplitude, consistent with the DJL theory discussed in §2.2 and also the dispersive two-layer theory of Esler & Pearce (2011). To further illustrate the link between the bore speed, C_b and nonlinear solitary waves, we have calculated the best-fit solitary wave solution to the DJL equation (2.1) and compared it to the leading wave at the bore front. These solutions are characterized by the wave speed and amplitude. They are also characterized by their Available Potential Energy, $APE = \int\int_0^{\eta(x,z)} b(z-\eta(x,z)) - b(z-\xi)d\xi dxdz$. For comparison, we calculate from simulations the APE at the bore front, between the ambient and the point of the first maximum, $h_{b_{max}}$. Because solutions to (2.1) are symmetric about the crest, we compare them with DJL solitary waves with an APE of twice this value. Results are shown in Figure 7 (left panels) for waves of increasing amplitude (increasing h_d) for $d_o = 0.2, \lambda = 8$. The results for bore speed as a function of bore amplitude, calculated through the first maximum for the simulations and through the wave crest for the DJL solutions, are shown in the right panels. Solutions that develop trapped cores (see §3.5) are extended in the core region using (3.11).

It is clear that the agreement is almost exact in the range where DJL solutions can be found. This illustrates that the bore speed is inherently linked to the waves at the front and the nonlinear DJL model is able to very accurately capture both the relationship $C_b(h_{b_{max}})$ and the shape of the front. The model we have introduced can be viewed as the function that connects $h_{b_{max}}$ to $\overline{h}_b$. The upstream condition sets the bore speed which then determines the characteristics of waves at the front, e.g. their amplitude and wavelength, and whether the bore is undular or monotonic/turbulent.

6. Discussion

Our results suggest that the waveguide established by the ambient stratification controls both the bore speed and the shape of the front. The small-amplitude limit of our continuous bore model is the linear equation governing normal modes, so the correct behavior is guaranteed (and observed) in that limit. In addition, for large amplitude, the bore models all converge to the energy-conserving conjugate state (independent of ϵ), and show good agreement with the simulations in that limit. We have chosen to terminate the curves at the conjugate state (since beyond it $D < 0$), however, some numerical simulations do result in larger amplitudes. In these cases, the speeds are well-approximated by the conjugate state speed, but a specific model does not exist. Previous results in two-layer systems (Baines 1995; White & Helfrich 2012) suggest that rarefactions may exist in this range.

The energy loss across the bore is complex, varying with both interface thickness and bore amplitude. However, two conclusions might be drawn. First, it is common for energy to be transferred to the lower denser layer from the upper regions (as demonstrated by Borden *et al.* 2012). Second, the dissipation appears to be greater than predicted by the KRS or CBWS-analog models, and is more consistent with the $\epsilon \to -\infty$ model. The success of this model for continuous stratification, suggests an improvement in the two-layer limit as compared with KRS or CBWS. Specifically, the bore speed from (3.6) in

the limit $\epsilon \to -\infty$ is given by

$$\frac{C_b}{(g'H)^{1/2}} = \left[\frac{d_o R^2(2d_oR + 2d_o - 2)(1 - d_oR)^2}{(6d_oR + 2d_o^2R^3 - 6d_o^2R^2 - R - 1)}\right]^{1/2}. \tag{6.1}$$

This curve is shown in Figure 8 along with the KRS and CBWS predictions and the simulation results for $\lambda = 64$ (the thinnest ambient interface studied here). While the continuous model is clearly more accurate, (6.1) provides a good approximation.

It is also important to note that the model we have introduced (as well as its two-layer limit) converges to the energy-conserving conjugate state solution. Previous work on two-layer bores has perhaps not sufficiently emphasized this large-amplitude limit, and the fact that the KRS, CBWS, Borden & Meiburg (2013) vorticity conservation model (and the more general arbitrary ϵ model we discuss) all converge to the same solution for $D = 0$. In our opinion this limit is an important feature, as it is the limiting amplitude for nonlinear internal waves.

7. Conclusions

We have presented a model for the speed of an internal bore in continuous stratification of arbitrary form. The model does require an assumption about dissipation, but we have demonstrated a closure which consistently produces good agreement with simulation results. Although a numerical solution is required, it can be carried out by straightforward eigenvalue techniques. In addition to matching the front speed from Navier-Stokes simulations, the model, by interpreting internal bores in terms of the nonlinear internal waveguide for the ambient stratification, gives physical insight into characteristics of the bore front. We hope this model will be of use for field observations of internal bores and nonlinear internal waves.

This work was supported by National Science Foundation grant OCE-1029672.

REFERENCES

Baines, P. G. 1995 *Topographic Effects in Stratified Flows*. Cambridge University Press.

Bell, J. B. & Marcus, D. L. 1992 A second-order projection method for variable-density flows. *J. Comp. Phys.* **101**, 334–348.

Benjamin, T. 1968 Gravity currents and related phenomena. *J. Fluid Mech.* **31**, 209–248.

Borden, Z. & Meiburg, E. 2013 Circulation-based models for boussinesq internal bores. *J. Fluid Mech.* **726**.

Borden, Z., Meiburg, E. & Constantinescu, G. 2012 Internal bores: An improved model via a detailed analysis of energy budget. *J. Fluid Mech.* **703**, 279–314.

Brown, D. J. & Christie, D. R. 1998 Fully nonlinear solitary waves in continuously stratified incompressible Boussinesq fluids. *Physics of Fluids* **10**, 2569–2586.

Chu, V. & Baddour, R. 1977 Surges, waves and mixing in two-layer density stratified flow. *Proc. 17th Congr. Intl. Assn. Hydraul. Res.* **1**, 303–310.

Cummins, P., Vagle, S., Armi, L. & Farmer, D. 2003 Stratified flow over topography: upstream influence and generation of nonlinear internal waves. *Proc. R. Soc. Lond. A* **459**.

Dubreil-Jacotin, M. 1934 Sur la determination rigoureuse des ondes permanentes periodiques damplitude finie. *J. Math. Pure Appl.* **13**, 217–291.

Esler, J. G. & Pearce, J. D. 2011 Dispersive dam-break and lock-exchange flows in a two-layer fluid. *J. Fluid Mech.* **667**, 555–585.

Helfrich, K. & White, B. 2010 A model for large-amplitude internal solitary waves with trapped cores. *Nonlin. Processes Geophys.* **17**, 303–318.

King, S. E., Carr, M. & Dritschel, D. G. 2010 The steady-state form of large-amplitude internal solitary waves. *J. Fluid Mech.* **666**, 477–505.

Klemp, J., Rotunno, R. & Skamarock, W. 1997 On the propagation of internal bores. *J. Fluid Mech.* **331**, 81–106.

Lamb, K. 2000 Conjugate flows for a three-layer fluid. *Physics of Fluids* **12**, 2169.

Lamb, K. & Wilkie, K. P. 2004 Conjugate flows for waves with trapped cores. *Phys. Fluids* **16**, 4685–4695.

Lamb, K. G. 2002 A numerical investigation of solitary internal waves with trapped cores formed via shoaling. *J. Fluid Mech.* **451**, 109–144.

Lamb, K. G. & Wan, B. G. 1998 Conjugate flows and flat solitary waves for a continuously stratified fluid. *Physics of Fluids* **10**, 2061–2079.

Li, M. & Cummins, P. 1998 A note on hydraulic theory of internal bores. *Dyn. Atmos. Oceans* **28** (1), 1–7.

Long, R. 1953 Some aspects of the flow of stratified fluids, i. a theoretical investigation. *Tellus* **5**, 42–57.

Marino, B., Thomas, L. & Linden, P. 2005 The front condition for gravity currents. *J. Fluid Mech.* **536**, 49–78.

Nash, J. D. & Moum, J. N. 2005 River plumes as a source of large-amplitude internal waves in the coastal ocean. *Nature* **437**, 400–403.

Pineda, J. 1999 Circulation and larval distribution in internal tidal bore warm fronts. *Limnol. Oceano.* **44**, 1400–1414.

Pratt, L. J. & Whitehead, J. A. 2008 *Rotating Hydraulics*. Springer.

Rottman, J. & Simpson, J. 1989 The formation of internal bores in the atmosphere - a laboratory model. *Quarterly Journal of The Royal Meteorological Society* **115**, 941–963.

Stastna, M. & Lamb, K. 2002 Large fully nonlinear internal solitary waves: The effect of background current. *Phys. Fluids* **14**, 2987–2999.

White, B. L. & Helfrich, K. R. 2008 Gravity currents and internal waves in a stratified fluid. *J. Fluid Mech.* **616**, 327–356.

White, B. L. & Helfrich, K. R. 2012 A general description of a gravity current front propagating in a two-layer stratified fluid. *J. Fluid Mech.* **711**.

Whitham, G. B. 1974 *Linear and Nonlinear Waves*. Wiley.

Wood, I. & Simpson, J. 1984 Jumps in layered miscible fluids. *J. Fluid Mech.* **140**, 215–231.

Yih, C. S. & Guha, C. R. 1955 Hydraulic jumps in a fluid system of two layers. *Tellus* **7**, 358–366.

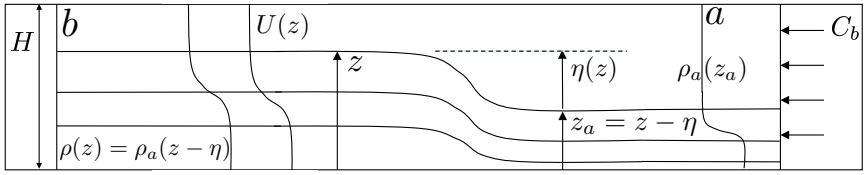

Figure 1: Schematic for an internal bore in continuous stratification. Velocity and density profiles are $U(z)$ and $\rho(z)$, where z is the vertical coordinate through the bore region. The isopycnal displacement, $\eta(z)$ is measured relative to the upstream ambient, where the density profile is $\rho_a(z-\eta)$. The bore speed is C_b.

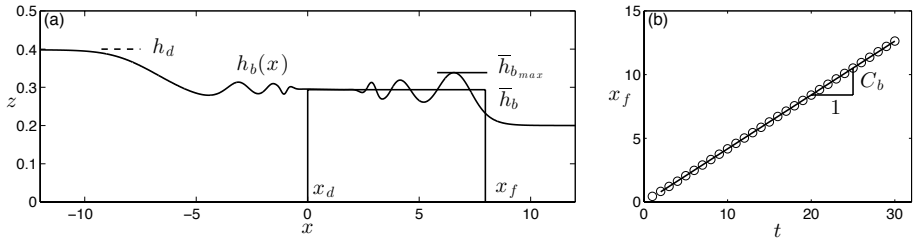

Figure 2: Internal bore properties from numerical simulations ($h_d = 0.4$, $d_o = 0.2$, $\lambda = 12$ shown as an example). **(a)** Bore height, $h_b(x)$ and mean value $\overline{h}_b$, taken between the initial dam location, x_d, and the front position, x_f ($t = 20$). Bore height at the location of the first maximum is $\overline{h}_{b_{max}}$. **(b)** Bore speed, C_b, obtained by linear regression of front position vs. time.

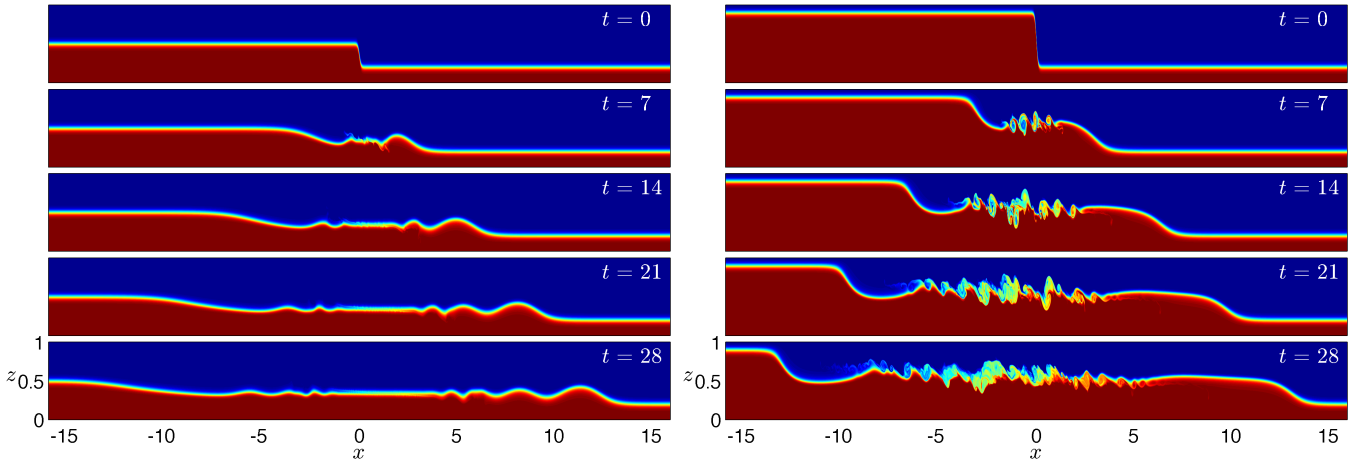

Figure 3: Results from dam-break simulations shown at different times. (a) undular bore ($h_d = 0.5$, $d_o = 0.2$, $\lambda = 24$). (b) turbulent bore ($h_d = 0.9$, $d_o = 0.2$, $\lambda = 24$). Color shows density.

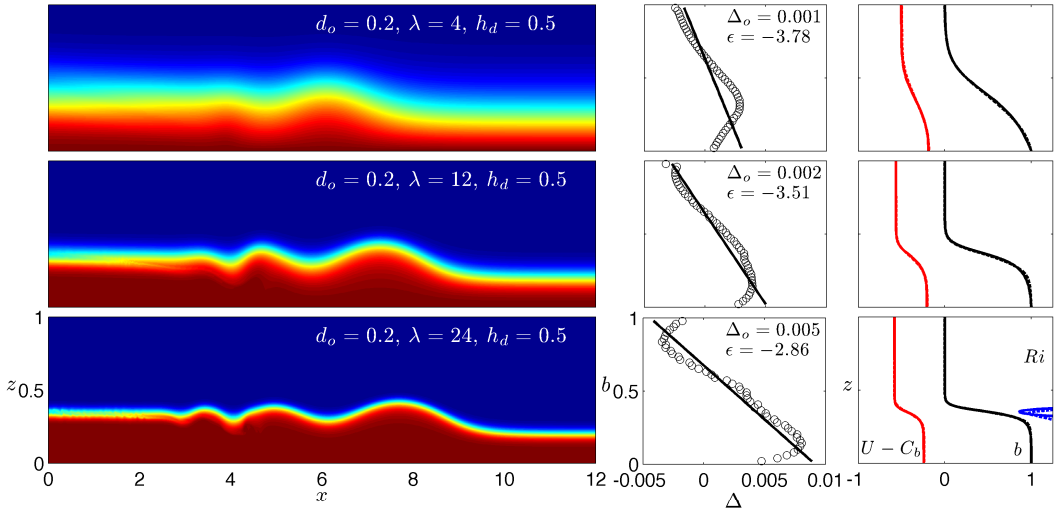

Figure 4: Undular bores with varying interface thickness, λ. Left panels: density field. Middle panels: mean head loss in isopycnal coordinates, from simulations (symbols) and with the best-fit linear profile based on (3.5) (solid line), with ϵ and Δ_o based on the fit. Right panels: velocity, density, and Richardson number profiles from model, with $\epsilon \to -\infty$ (solid lines), and simulations (dashed lines).

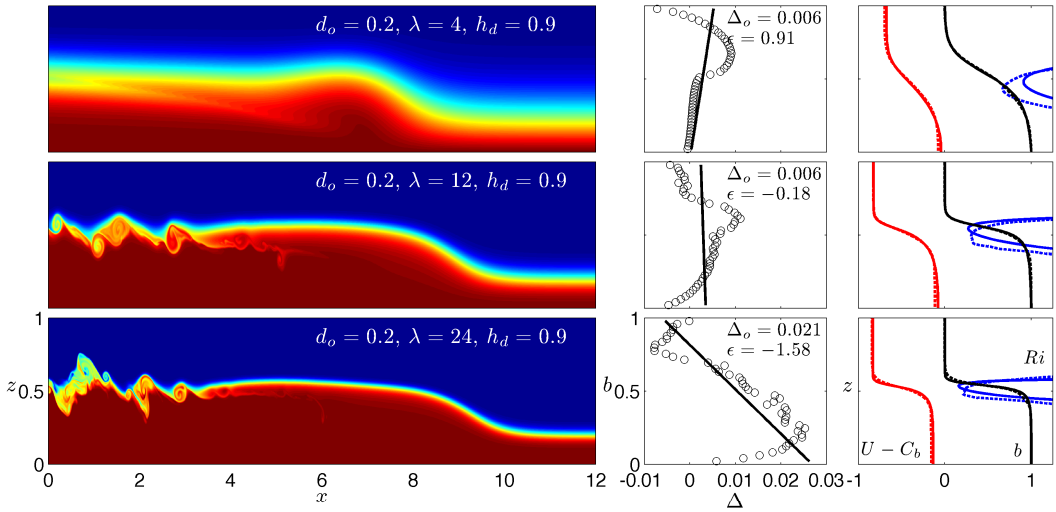

Figure 5: Turbulent (monotonic) bores with varying λ. Details are as described in figure 4.

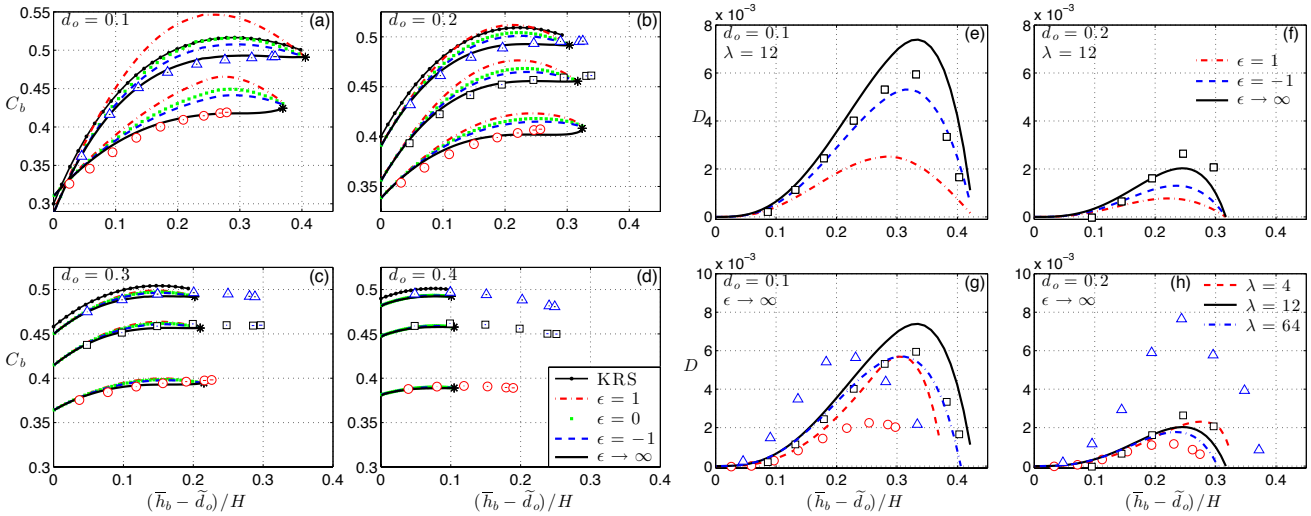

Figure 6: Comparison between model and theory for bores with varying ambient stratification. Left panels $(a-d)$: bore speed vs. amplitude. Right panels $(e-h)$: dissipation vs. amplitude. In each panel, symbols (with error bars) represent numerical results: $\lambda = 4$ ($\circ$), $\lambda = 12$ ($\square$), $\lambda = 64$ ($\triangle$). Curves show the theoretical results for varying ϵ and λ (see legends). In (a-d), $*$ denotes the energy-conserving conjugate state.

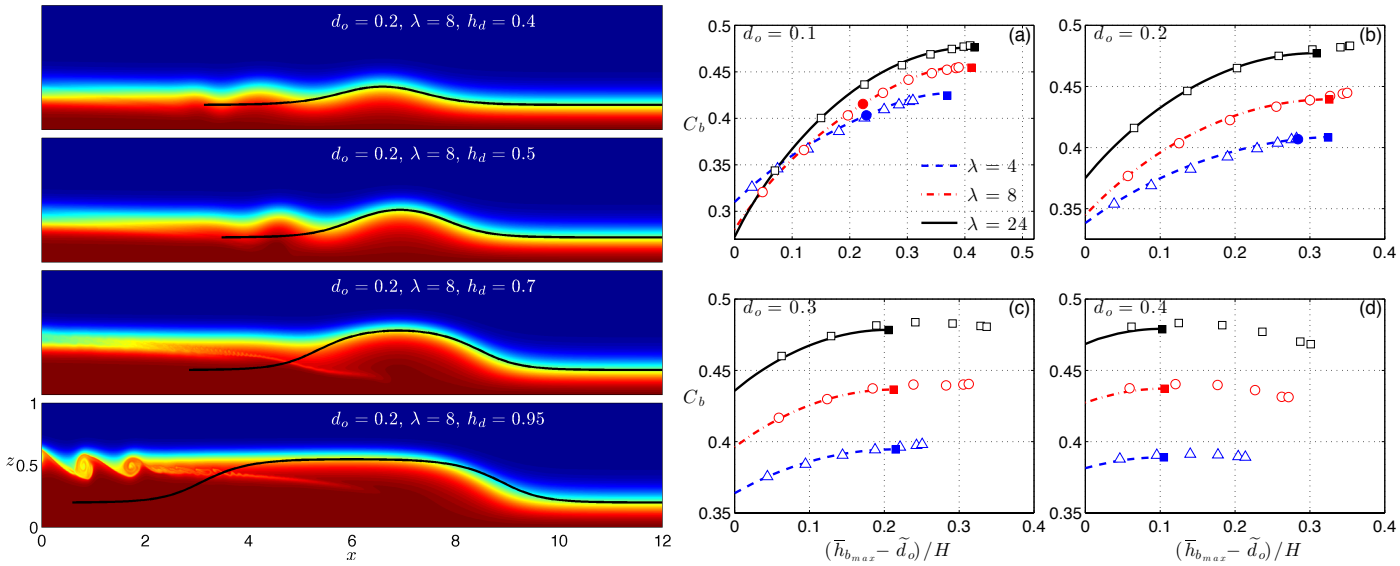

Figure 7: Characteristics of the bore front. Left panels: density field from simulations for bores of increasing amplitude (color) and the $b = 0.5$ isopycnal from the 2D DJL solution (line), obtained by matching APE for $x \geq h_{b_{max}}$. Right panels: bore speed vs. amplitude at the first maximum, $h_{b_{max}}$. Open symbols: numerical results. Curves: DJL theory. Solid squares: conjugate state. Solid circles: onset of trapped core solutions.

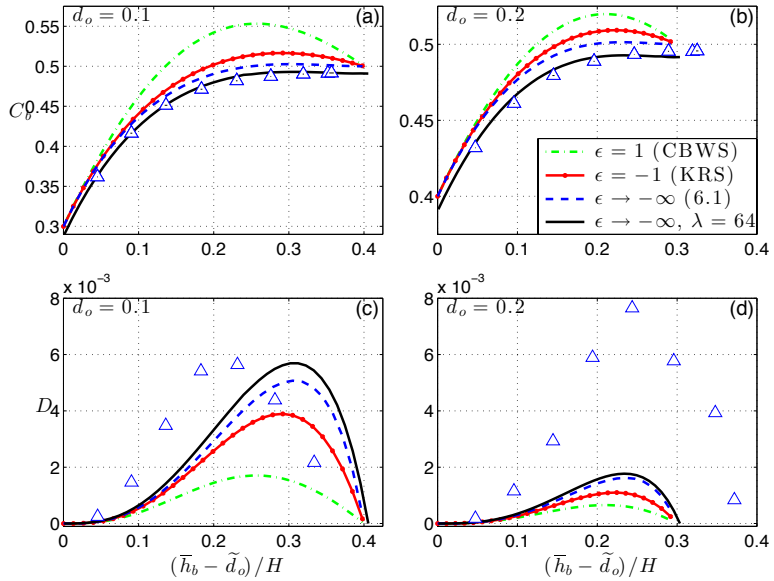

Figure 8: Comparison between two-layer bore theories and thin-interface numerical results ($\lambda = 64$). $(a - b)$: bore speed vs. amplitude. $(c - d)$: dissipation vs. amplitude.